Testing the relativistic Doppler boost hypothesis for the binary candidate quasar PG1302-102 with multiband *Swift* data

Chengcheng Xin,[1] Maria Charisi,[2]★ Zoltán Haiman,[1] David Schiminovich,[1] Matthew J. Graham [ORCID],[2] Daniel Stern[3] and Daniel J. D'Orazio[4]

[1]*Department of Astronomy, Columbia University, New York, NY 10027, USA*
[2]*Division of Physics, Mathematics and Astronomy, California Institute of Technology, Pasadena, CA 91125, USA*
[3]*Jet Propulsion Laboratory, California Institute of Technology, Pasadena, CA 91109, USA*
[4]*Department of Astronomy, Harvard University, Cambridge, MA 02138, USA*

ABSTRACT

The bright quasar PG1302-102 has been identified as a candidate supermassive black hole binary from its near-sinusoidal optical variability. While the significance of its optical periodicity has been debated due to the stochastic variability of quasars, its multiwavelength variability in the ultraviolet (UV) and optical bands is consistent with relativistic Doppler boost caused by the orbital motion in a binary. However, this conclusion was based previously on sparse UV data that were not taken simultaneously with the optical data. Here, we report simultaneous follow-up observations of PG1302-102 with the Ultraviolet Optical Telescope on the *Neil Gehrels Swift Observatory* in six optical + UV bands. The additional nine *Swift* observations produce light curves roughly consistent with the trend under the Doppler boost hypothesis, which predicts that UV variability should track the optical, but with a ∼2.2 times higher amplitude. We perform a statistical analysis to quantitatively test this hypothesis. We find that the data are consistent with the Doppler boost hypothesis when we compare the the amplitudes in optical *B*-band and UV light curves. However, the ratio of UV to *V*-band variability is larger than expected and is consistent with the Doppler model, only if either the UV/optical spectral slopes vary, the stochastic variability makes a large contribution in the UV, or the sparse new optical data underestimate the true optical variability. We have evidence for the latter from comparison with the optical light curve from All-Sky Automated Survey for Supernovae. Additionally, the simultaneous analysis of all four bands strongly disfavours the Doppler boost model whenever *Swift V* band is involved. Additional, simultaneous optical + UV observations tracing out another cycle of the 5.2-yr proposed periodicity should lead to a definitive conclusion.

Key words: quasars: individual: PG1302-102 – quasars: supermassive black holes.

1 INTRODUCTION

It is well established that all massive galaxies host supermassive black holes (SMBHs), with masses 10^6–$10^{10} M_\odot$, in their nuclei (Kormendy & Ho 2013). According to cosmological models of structure formation, galaxies merge frequently to form more massive galaxies (e.g. Haehnelt & Kauffmann 2002). It follows that compact SMBH binaries (SMBHBs) should be common in galactic nuclei (Begelman, Blandford & Rees 1980). As a by-product of galaxy mergers, SMBHBs are important for understanding galaxy evolution. They are also important because at small (milli-parsec)

separations, they become strong sources of low-frequency gravitational waves (GWs), and are the prime targets for experiments such as the Pulsar Timing Arrays (PTAs; e.g. Burke-Spolaor et al. 2019) and the *Laser Interferometer Space Antenna (LISA)*.[1]

Despite their expected ubiquity, observational evidence, especially for compact sub-parsec SMBHBs, remains sparse (De Rosa et al. 2019). Dual AGN at kpc separations have been repeatedly resolved in X-rays, optical and infrared (Komossa et al. 2003; Comerford et al. 2011), but as the SMBHs move to smaller separations, they can only be resolved in radio bands, with Very Long Baseline Interferometry (VLBI; e.g. Rodriguez et al. 2006). At

---

★ E-mail: mcharisi@caltech.edu

[1]See http://lisamission.org.

sub-parsec separations, they are practically below the resolution limits of even VLBI (although see D'Orazio & Loeb 2017). Therefore, the presence of a binary needs to be inferred indirectly from its effect on the surrounding matter.[2]

One proposed method to identify SMBHBs is to search for periodic variability in quasars. The intuitive expectation that the orbit of the SMBHB will periodically perturb the nearby gas has been confirmed in multiple hydrodynamical simulations. Overall, the emerging picture is that the binary evacuates a central cavity in the disc, while gaseous streams enter the cavity periodically and efficiently accrete on to the SMBHs (Artymowicz & Lubow 1996; MacFadyen & Milosavljević 2008; Cuadra et al. 2009; Roedig et al. 2011; Nixon et al. 2011; Roedig et al. 2012; D'Orazio, Haiman & MacFadyen 2013; Gold et al. 2014). This likely results in bright quasar-like luminosity (possibly, repeating bursts), which is periodically modulated at roughly the orbital period of the binary, with the structure of the periodogram depending strongly on the mass ratio (see e.g. Farris et al. 2014; Shi & Krolik 2015; D'Orazio et al. 2016).

Additionally, some of the incoming gas becomes bound to the SMBHs, creating mini-discs around each SMBH (Ryan & MacFadyen 2017; Tang, MacFadyen & Haiman 2017). In compact binaries, the SMBHs move at relativistic speeds, and thus the emission from the mini-discs, and in particular, the emission of the secondary mini-disc (which is expected to be brighter and has a higher orbital velocity) is Doppler boosted. Since the thermal disc emission is radially stratified, with higher energy emission arising from smaller radii, the expectation is that at higher frequencies, this Doppler effect is increasingly important, and becomes dominant above frequencies corresponding to thermal emission from the outer edges of the mini-discs (roughly coinciding with the *V* band in the case of PG1302-102; see D'Orazio, Haiman & Schiminovich 2015b). For typical spectral slopes $\alpha_\nu \equiv \mathrm{d}\ln F_\nu/\mathrm{d}\ln \nu < 3$ the binary will appear brighter/dimmer, when the secondary SMBH is approaching/receding from the observer, even if the rest-frame luminosity is constant. To first order in orbital velocity and for a power-law spectrum, the observed flux is modulated as

$$\frac{\Delta F_\nu}{F_\nu} = (3 - \alpha_\nu)\frac{v}{c}\cos\phi\sin i, \tag{1}$$

where v is the orbital velocity of the more luminous SMBH (with the other BH assumed to be much dimmer), i is the inclination of the orbit with respect to the line of sight, and ϕ is the orbital phase. For unequal-mass binaries that are not too far from edge-on, the Doppler boost may dominate the variability, producing a smooth quasi-sinusoidal light curve.

Systematic searches for quasars with periodic variability in time-domain surveys, e.g. the Catalina Real-Time Transient Survey (CRTS), the Palomar Transient Factory, and the Panoramic Survey Telescope and Rapid Response System have identified ∼150 binary candidates (Graham et al. 2015a; Charisi et al. 2016; Liu et al. 2019).[3] However, the stochastic variability of quasars can introduce spurious detections. This is further aggravated by our incomplete understanding of the precise form of intrinsic quasar variability

(Vaughan et al. 2016) coupled with the relatively short baselines, in which only a few cycles can be observed. Indeed, several recent studies have found inconsistencies with the widely used damped random walk (DRW) models, and favoured other descriptions of stochastic quasar variability (e.g. Mushotzky et al. 2011; Caplar, Lilly & Trakhtenbrot 2017; Smith et al. 2018). Throughout our analysis, we here nevertheless follow Graham et al. (2015a) and Charisi et al. (2016), who explicitly included stochastic noise in their statistical analysis by assuming that quasar variability is described by a DRW model.

Sesana et al. (2018) demonstrated that the samples of quasars with periodic variability likely contain many false positives. They found that the GW background inferred from this population of binary candidates is in tension with the PTA upper limits. On the other hand, theoretical models predict that at least a few closely separated SMBHBs should be detectable in the current time-domain surveys (Haiman, Kocsis & Menou 2009; Kelley et al. 2019). It is thus crucial to select the genuine binaries among the candidates by identifying additional binary signatures, such as multiple components of periodic variability (Charisi et al. 2015; D'Orazio et al. 2015a), self-lensing flares (D'Orazio & Di Stefano 2018), or the wavelength dependence of the Doppler modulation (D'Orazio et al. 2015b; Charisi et al. 2018).

Among the identified candidates, a prominent source from the CRTS sample is quasar PG1302-102 (Graham et al. 2015b). It is a bright quasar at redshift $z = 0.27$ with a BH mass of $\sim 10^9\,\mathrm{M_\odot}$. It exhibits quasi-sinusoidal variability with a period of ∼5.2 yr and an amplitude of ∼0.14 mag in *V* band. The significance of the periodicity has been a topic of controversy; Vaughan et al. (2016) with a Bayesian analysis showed that the DRW model is preferred to a sinusoid, whereas D'Orazio et al. (2015b) with a similar approach reached the opposite conclusion.[4] Charisi et al. (2015) also found the periodogram peak to be significant, but only considering it as a stand-alone detection (i.e. trial factors, to account for the fact that PG1302-102 was chosen from a large sample, were not included). Recently, Liu, Gezari & Miller (2018) added data from the All-Sky Automated Survey for Supernovae (ASAS-SN) and found that a sinusoidal + DRW model is preferred to a pure DRW model, but the significance of the periodicity decreased.[5] Undoubtedly, long-term monitoring will determine whether the periodicity of PG1302-102 is persistent.

Beyond the simple periodicity, D'Orazio et al. (2015b, *hereafter* DHS15) suggested that the multiwavelength variability of PG1302-102 is consistent with relativistic Doppler boost, serving as an additional indication for its binary nature.[6] More specifically, in the Doppler boost scenario described above, there is a robust multiwavelength prediction: if the UV luminosity also arises in the mini-discs, the optical and UV light curves should vary in tandem. The variability amplitudes A_{UV}, A_{opt} depend on the respective spectral indices α_{UV}, α_{opt} (equation 1), which means that the relative

---

[2]We also note that, in the (not-too-distant) future, compact binaries will be directly 'observable' in GWs with PTAs and *LISA*.

[3]Additional candidates have also been identified individually (Bon et al. 2016; Zheng et al. 2016; Dorn-Wallenstein, Levesque & Ruan 2017; Li et al. 2019), although the statistical significance of the latter was brought into question by Barth & Stern (2018).

[4]The different conclusions are possibly due to the dramatically different best-fitting τ parameters for the DRW model.

[5]The light curve from ASAS-SN has inferior photometric quality compared to CRTS. Also, the binning of the light curve may significantly affect the statistical analysis. Liu et al. (2018) chose wide bins of 150 d, longer than the typical DRW time-scale.

[6]Further signatures for the binary nature of PG1302-102 have been suggested; for instance, its variability in the mid-infrared is quasi-sinusoidal (Jun et al. 2015), and the angle of its radio jet varies roughly at the proposed optical 5.2-yr period, (Qian et al. 2018).

amplitudes in the two bands are

$$\frac{A_{\mathrm{UV}}}{A_{\mathrm{opt}}} = \frac{3 - \alpha_{\mathrm{UV}}}{3 - \alpha_{\mathrm{opt}}}. \tag{2}$$

The model prediction was tested with UV spectra and photometry from the *Hubble Space Telescope (HST)* and the *GALaxy Evolution EXplorer (GALEX)*. However, the UV data were quite sparse in DHS15. Subsequently, Charisi et al. (2018) demonstrated in a sample of non-periodic quasars that, with the currently available sparse UV data, the multiwavelength Doppler signature can be confused with wavelength-dependent variability of quasars. The probability that the multiwavelength Doppler boost signature arises by chance increases as the quality of the UV data decreases (e.g. from 20 per cent in the near-UV sample to ~40 per cent in the far-UV sample–see also figs 2 and 3 in Charisi et al. 2018). These probabilities reflect the limited quality of the data in the control samples, and represent only upper limits on how frequently quasars mimic the Doppler brightness+colour variations by chance.

Motivated by this, we obtained multiwavelength follow-up data with the Ultraviolet/Optical Telescope (UVOT), on-board the *Neil Gehrels Swift Observatory*. In this paper, we report the new observations and further test the Doppler boost hypothesis by examining whether UV variability tracks that of the optical, but with a larger amplitude. We assume that the variability of PG1302-102 consists of a sinusoidal modulation caused by the relativistic Doppler boost with UV and optical amplitudes defined by the spectral slopes in each band, as well as stochastic DRW variability with amplitudes that may differ in each band, and photometric noise. We confront this model with new data points that we acquired in two optical and two *UV* bands at nine distinct epochs. With simulations, we assess the probability that the data are consistent with the Doppler boost model by comparing the UV/optical variability ratios.

The rest of this paper is organized as follows. In Section 2, we describe the new *Swift* data, and the details of our statistical analysis. In Section 3, we present the results of our statistical tests, which are discussed further in Section 4. We summarize our main conclusions in Section 5.

2 DATA ANALYSIS

2.1 Data

We obtained multiwavelength observations of PG1302-102 with the UVOT on *Swift*, initially as a Target of Opportunity, and subsequently, through two approved Guest Observer programs in Cycles 13 and 14 (PI: Z. Haiman). We extracted the *Swift* light curves using the *On-line XRT & UVOT data analysis* pipeline.[7] Our observations cover all six filters of UVOT (*B* and *V* in optical, *W*2, *M*2, *W*1, and *U* in UV). We include one additional archival observation, which also covers all six bands. The photometric measurements of the *Swift* optical and *UV* bands are reported in Table A1 in Appendix A.

In Fig. 1, we present the optical and near-UV light curves of PG1302-102 from our monitoring campaign with *Swift*/UVOT, along with archival data from other surveys. More specifically, in the top panel, we show the optical light curve from Graham et al. (2015b) in black, the ASAS-SN light curve,[8] which was analysed in

Liu et al. (2018) in grey. The *Swift* observations are superimposed with purple squares for *B* band and red diamonds for *V* band. The ASAS-SN and *Swift* V-band light curves are calibrated in the same photometric system and are directly comparable (see Section 4.1), whereas for the light curve from Graham et al. (2015b), a constant shift is necessary. We calculated this offset from the difference of the mean magnitudes in the overlapping time interval.

In the bottom panel, we present the near-UV data from DHS15 (the black circles and the triangles for *GALEX* and *HST* observations, respectively) and the *Swift* data points with red diamonds for *M*2 band and purple squares for *W*1 band. Similar to the optical, we apply a constant offset based on the two *Swift* data points that are almost coincident in time with the *GALEX/HST* observations (at MJD ~ 54 500). We also show the sinusoidal model for relativistic Doppler boost using the best-fitting orbital parameters from DHS15.

We note that the *Swift* V and *M*2 bands have very similar wavelength coverage to the optical and near-*UV* bands examined in DHS15 (see Figs 5 and 6 next). This allows us to directly compare the new observations with the archival data. It also justifies the choice of a constant offset for the calibration of the different pieces of the time series, since the colour-dependent variability of quasars should have minimal impact in the almost identical filters.

As can be seen from Fig. 1, the *Swift* data cover a total of nine epochs, separated by approximately 3-4 months (over the past 2 yr of our monitoring campaign) and span a baseline of ~1770 d. A key characteristic of our observations is that the data in the distinct filters were taken nearly simultaneously. This is crucial because quasars show short-term fluctuations. In previous work, this presented a limitation, since the UV data had to be compared with the extrapolated optical variability. For this reason, we exclude from the analysis a few archival observations that cover only one band. The simultaneous coverage allows more flexibility to test the Doppler hypothesis, beyond the simplest assumption of sinusoidal variability, which corresponds to constant luminosity in the mini-discs. From hydrodynamic simulations, we expect fluctuations in the accretion rate on shorter time-scale than the orbital period, and thus the intrinsic luminosity of the mini-discs likely may deviate from constant (Farris et al. 2014).

2.2 Analysis

The relativistic Doppler boost model predicts the modulation of the observed flux (equation 1). In the limit of small fluctuations [a reasonable approximation for PG1302-102's O(10 per cent) variability], to first order the additive magnitude variation is $\Delta m \equiv m - m_0 = \Delta F / F_0$. In other words, the fractional change in flux and the change in the apparent magnitude are equivalent. We adopt this approximation for the rest of the paper.

We want to test whether the optical/UV variability of PG1302-102 follows the multiwavelength prediction of the relativistic Doppler model, i.e. the optical and UV light curves vary simultaneously, with amplitudes according to equation (2). Our null hypothesis is that the observations are consistent with Doppler boost plus DRW variability. The former reflects the emission of the binary orbiting with relativistic speed, whereas the latter represents additional variability from accretion processes in the quasar.

We quantify the relative change in magnitude between two bands (e.g. *V* and *M*2), by taking the ratio of the magnitude difference between two observations, i and j (at times t_i and t_j, respectively).

$$R_{\mathrm{ij}} = \frac{\Delta V_{\mathrm{ij}}}{\Delta M2_{\mathrm{ij}}} = \frac{V(t_i) - V(t_j)}{M2(t_i) - M2(t_j)}. \tag{3}$$

---

[7]http://www.ssdc.asi.it/mmia/index.php?mission=Swiftmastr
[8]We extracted the ASAS-SN light curve from the on-line data base *Sky Patrol* (Shappee et al. 2014; Kochanek et al. 2017).
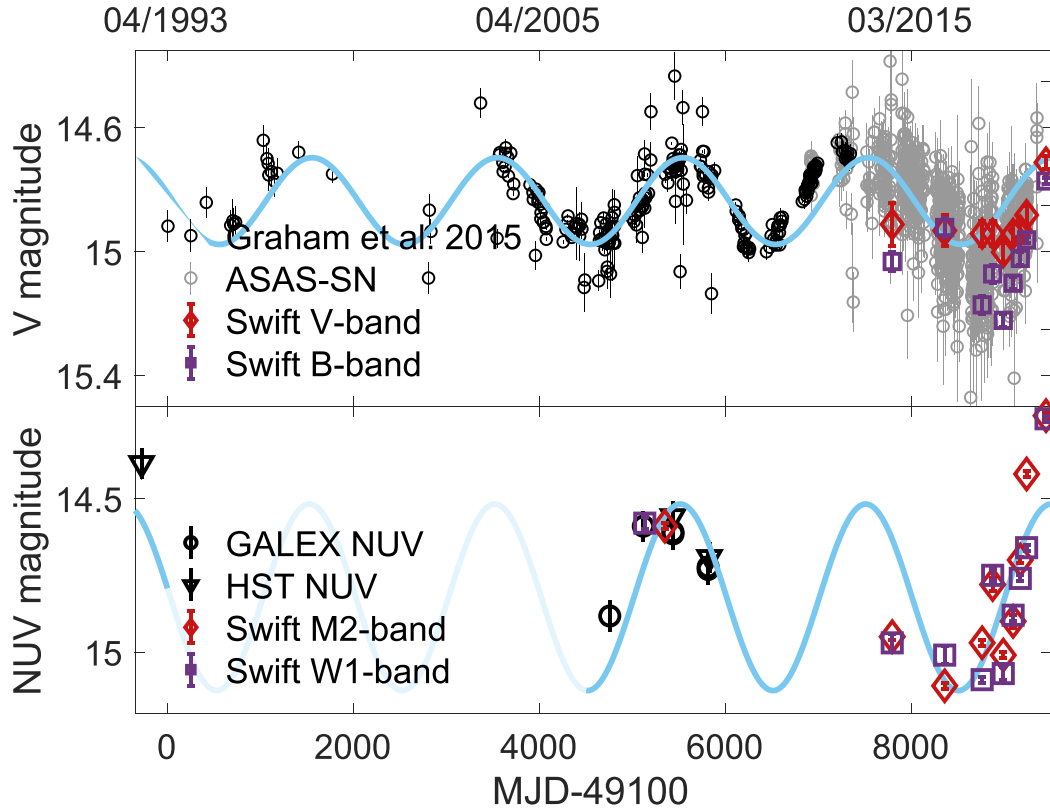
Figure 1. Top Panel: optical light curve of PG1302-102 with data from Graham et al. (2015b) in black (CRTS+LINEAR and other archival observations), data from ASAS-SN in grey, and the purple squares/red diamonds for *Swift B/V*-band observations. Bottom panel: near-UV light curve, with the black circles and the triangles for *GALEX* and *HST* observations, respectively, from DHS15 and the purple squares and the red diamonds for *Swift W*1 and *M*2-band observations, respectively. The sinusoidal Doppler boost model from DHS15 is also shown in light blue.

We consider the differences between all possible combinations of data points; with nine distinct observations from *Swift*, there are 36 total combinations (without repetition). As equation (3) implies, we first examine the *V* and *M*2 bands for comparison with DHS15 (see Section 1), but subsequently we consider multiple combinations of bands. Also, in this analysis, we did not include the archival observations from DHS15 because the optical and UV data were not taken simultaneously.

Introducing the ratio R_{ij} as a metric for the relative change in variability is advantageous for the following reasons. First, unlike a least-squares fit (or any other similar model fit), our approach does not explicitly make an assumption about the shape of the periodicity. As a result, deviations from a sinusoid, e.g. due to an eccentric binary orbit, fluctuations in the luminosity of the mini-discs, or significant gas motions contributing to the Doppler effect on top of the binary's orbital motion (Tang, Haiman & MacFadyen 2018) are automatically incorporated. Additionally, fitting a model with multiple parameters when we only have nine observations can be problematic (e.g. susceptible to outliers). Another significant advantage is that we do not need to subtract the uncertain mean magnitude in each band. This is especially important in our case because in addition to having a limited number of observations, we preferentially sample the dim phase of the periodicity. We note that even though the baseline of the *Swift* observations is ∼1770 d, close to the detected period of PG1302-102, our dedicated monitoring in Cycles 13 and 14 covers only 2 yr.

In the most idealized case of Doppler boost emission (i.e. constant luminosity of the mini-discs, without any extra intrinsic variability (e.g. DRW) from the quasar, and perfect observations without

photometric errors), the ratio R_{ij} would be exactly constant and equal to $(3 - \alpha_V)/(3 - \alpha_{M2})$, which for the *V* and *M*2 bands is 1/2.17 (DHS15). However, both the photometric errors and the DRW variability add scatter around the expected value, producing a distribution of R_{ij} values.

In order to assess whether the observed distribution is consistent with the null hypothesis, we simulate light curves with Doppler boost variability plus a DRW component:

$$V = V_{DB} + V_{DRW} \quad \text{and} \quad M2 = M2_{DB} + M2_{DRW}. \qquad (4)$$

We first assume the simplest model for relativistic Doppler boost, i.e. constant luminosity in the rest frame of the SMBH, which gives rise to a sinusoidal light curve. Therefore, $V_{DB} = A_V \sin(2\pi t/P + \phi)$ and $M2_{DB} = A_{DB} \times V_{DB}$, where $A_{DB} = (3 - \alpha_{M2})/(3 - \alpha_V)$. For our fiducial model, we set $P = 1994$ d, $A_V = 0.14$ mag, $\phi = \pi$, and $A_{DB} = 2.17$, following DHS15.

For the DRW light curves, we use the power spectral distribution (PSD) from Kozłowski et al. (2010),

$$PSD(f) = \frac{2\sigma^2 \tau^2}{1 + (2\pi f \tau)^2}, \qquad (5)$$

with $\sigma = 0.071$ mag$/\sqrt{d}$ and $\tau = 48$ d from DHS15.[9] Using the prescription from Timmer & Koenig (1995), numerically implemented in python in the ASTROML package (Vanderplas et al. 2012; Ivezić

---

[9] As mentioned above, the best-fitting DRW parameters of PG1302-102 reported in the literature have a wide range. Next, we explore a range of values that cover the published results.
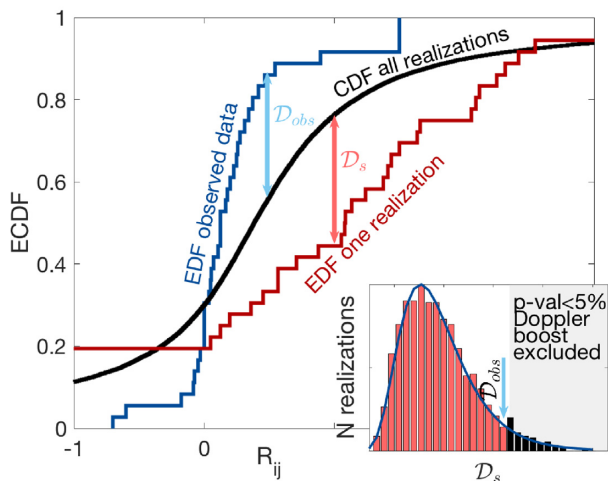
Figure 2. Illustration of the test statistic and the calculation of the *p*-value of the null hypothesis.

et al. 2014), we generate evenly sampled DRW time series with a cadence of 1 d. We downsample the data at the observed times and add Gaussian errors, with zero mean and standard deviations equal to the photometric errors, in order to generate light curves with properties similar to the observations. We assume that the DRW model has similar amplitudes in optical and UV, i.e. $\sigma_{\rm opt} = \sigma_{\rm UV}$ (but relax this assumption next). We generate a distribution of $R_{\rm ij}$ by simulating 1000 mock light curves.

We test the null hypothesis (i.e. the multiwavelength light curves are consistent with the relativistic Doppler boost plus DRW model) by examining whether the distribution of $R_{\rm ij}$ from the observed light curve $R_{\rm obs}$ is drawn from the same distribution as the simulated data $R_{\rm s}$. Typically, a Kolmogorov–Smirnov (KS) test is performed. However, the KS test assumes that the measurements are independent and identically distributed, which is not true for $R_{\rm ij}$, since we use multiple pairwise combinations of the same data points.

We overcome this limitation by employing the basic principle of the KS test, while accounting for the fact that the values $R_{\rm ij}$ are not independent. More specifically, the KS test quantifies the difference between a sample and a reference distribution with the maximum distance $\mathcal{D}$ between the empirical distribution function (EDF) of the sample and the cumulative distribution function (CDF) of the reference distribution. Confidence limits are then commonly obtained from approximate or asymptotic distributions of the distance $\mathcal{D}$ between independent realizations of the reference distribution. We here consider the distribution of $R_{\rm s}$ from all simulated realizations as the reference distribution, and similar to the KS test, we define $\mathcal{D}_{\rm obs}$, the maximum distance between the EDF of $R_{\rm obs}$ and the CDF of $R_{\rm s}$ as our test statistic. However, we then explicitly compute the null distribution (i.e. the distribution of the test statistic) from the simulated data by calculating the maximum distance $\mathcal{D}_{\rm s}$ between the EDF of each realization and the CDF of $R_{\rm s}$.

We define the *p*-value as the fraction of realizations that have maximum distance $\mathcal{D}$ greater than the observed ($\mathcal{D}_{\rm s} > \mathcal{D}_{\rm obs}$). Note that a small $\mathcal{D}$ value indicates good agreement between the sample and the reference distribution. If the *p*-value is less than 5 per cent, we can reject the null hypothesis at the 5 per cent level. If, on the other hand, the *p*-value is greater than 5 per cent, the evidence against the null hypothesis is weak, and the observations could be consistent with relativistic Doppler boost. In Fig. 2, we illustrate the

Table 1. Best-fitting DRW parameters from previous studies.

Reference	σ (mag/$\sqrt{d}$)	τ (d)
MacLeod et al. (2010)	0.01 (0.15 mag)	245
DHS15	0.071 (0.049 mag)	48
Charisi et al. (2015)	0.0157	~100
Vaughan et al. (2016)	0.004	550
Liu et al. (2018)[a]	0.005	429

[a]These parameters were calculated for the light curve that includes only LINEAR+CRTS data points. With the inclusion of the ASAS-SN data, the best-fitting parameters are $\sigma = 0.004$ mag/$\sqrt{d}$ and $\tau = 610$ d (T. Liu; private communication).

test statistic and the calculation of the *p*-value. In the completely idealized case [without any extra intrinsic variability (e.g. DRW)] from the quasar and without photometric errors], the CDF would be a step function at 0.46 (1/2.17).

Finally, we explore how the choice of parameters (namely, the DRW parameters σ and τ, the Doppler boost amplitude ratio $A_{\rm DB}$ and the relative amplitude of the intrinsic quasar variability in optical and UV $\sigma_{\rm opt}/\sigma_{\rm UV}$) affect our results. Specifically, we vary σ from 0.003 to 0.08 mag/$\sqrt{d}$ and τ from 30 to 500 d on a 10 × 10 linearly spaced grid to sufficiently cover the best-fitting parameters in Table 1, due to the their uncertainties.

3 RESULTS

3.1 Doppler boost test in the *V* and *M*2 bands

We test the multiwavelength Doppler boost signature for the binary candidate PG1302-102 with simultaneous optical and UV observations. For direct comparison with DHS15, we first test the light curves in *V* band (optical) and *M*2 band (UV)[10] adopting the parameters from their analysis. For the fiducial model, we find that only 47 realizations produce a maximum distance larger than the observed (*p*-value = 4.7 per cent), and thus we can reject the hypothesis that the data are consistent with the Doppler boost model.

As stated in Section 1, there is significant uncertainty with respect to the best-fitting DRW parameters for PG1302-102. For reference, we also calculate the expected values of σ and τ for a typical quasar with the luminosity and redshift of PG1302-102. For this, we use the equations from MacLeod et al. (2010):

$$\log(X) = A + B \log\left(\frac{\lambda/(1+z)}{4000\text{Å}}\right) + C(M_i + 23)$$
$$+ D \log\left(\frac{M_{\rm BH}}{10^9\,{\rm M}_\odot}\right), \tag{6}$$

with (A, B, C, D) = (2.4, 0.17, 0.03, 0.21) for $X = \tau_{\rm RF}$ and (A, B, C, D) = (−0.51, −0.479, 0.131, 0.18) for $X = \sqrt{2}\sigma$.

For PG1302-102, $M_{\rm BH} = 10^9{\rm M}_\odot$, $z = 0.27$, and for *V*-band $\lambda = 5402$ Å. The absolute *i*-band magnitude can be calculated directly from the optical/IR spectrum in Graham et al. (2015b); we calculate the (rest-frame) *i*-band flux, $F_i = 2 \times 10^{-13}$ erg cm^{-2} s^{-1} and convert it to an *i*-band luminosity and subsequently to absolute magnitude ($M_i = -23.2$). In Table 1, we summarize the values of σ and τ from previous studies, along with the estimated values from MacLeod et al. (2010).

The large range of reported best-fitting DRW values shown in Table 1 are likely responsible for the controversy regarding

---

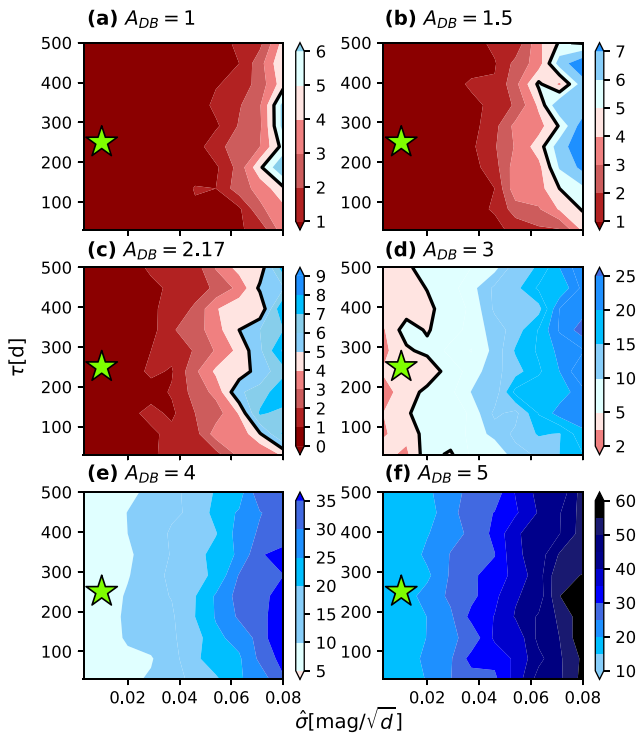[10]In Section 3.2, we extend the test to additional bands.

Figure 3. *P*-value (the colour bars; in unit of per cent) of the null hypothesis (i.e. the multiband light curves are consistent with Doppler boost plus DRW model) as a function of the DRW parameters σ and τ, with $A_{DB} = 1$ (top left), 1.5 (top right), 2.17 (middle left), 3 (middle right), 4 (bottom left), and 5 (bottom right) and UV/optical noise ratio $\sigma_{UV}/\sigma_{opt} = 1$, considering the *Swift V*- and *M*2-bands. The black solid line represents the 5 per cent *p*-value threshold, which separates models that are rejected (red) from those passing the test (blue). The star corresponds to the average σ and τ for quasars with properties similar to PG1302-102 from MacLeod et al. (2010).

the significance of PG1302-102's periodicity. The values are not directly comparable because each study used different components of the light curve of PG1302-102 (e.g. Vaughan et al. 2016 used only the CRTS data, Liu et al. 2018 used CRTS+LINEAR, whereas Charisi et al. 2015 and DHS15 analysed the full published light curve from Graham et al. 2015b) and somewhat different methods to constrain the DRW parameters. For instance, Liu et al. (2018) binned the light curve in very wide bins, which can significantly affect both the parameter estimation and the periodicity significance, as demonstrated with simulated data by Zhu & Thrane (2020). On the other hand, Vaughan et al. (2016) introduced a parameter to account for a bias in the photometric errors; using the light curve from Graham et al. (2015b) and without this extra parameter, the estimated DRW parameters were similar to Charisi et al. (2015) and S. Vaughan (private communication). Additionally, as Kozłowski (2017) demonstrated with simulated DRW light curves, it is particularly challenging to constrain the DRW parameters, especially when τ is relatively long compared to the baseline. Finally, the errors on the best-fitting values (especially on τ) are typically large. Therefore, the differences between the quoted best-fitting values of the DRW parameters is not surprising.

Because of this, we take an agnostic approach and test the Doppler boost model for a wide range of DRW parameters. Initially, we keep the parameters of the Doppler boost model as in DHS15. In Fig. 3 (top left-hand panel), we show the *p*-value of the null hypothesis as a function of σ and τ for $A_{DB} = 2.17$. We see that for typical

DRW parameters, we can reject that the data are consistent with the Doppler boost model, whereas for higher σ, the evidence against the Doppler model becomes weaker. In particular, at the fiducial $A_{DB} = 2.17$, the only allowed models are those with $\sigma \gtrsim 0.07$ mag/$\sqrt{d}$. At face value, this indicates that the DRW component of variability dominates, and is a better description of the data. For example, the study by Vaughan et al. (2016), which found the highest best-fitting values for the DRW parameters, questioned the significance of the periodicity; they concluded that the DRW model is preferred to a purely sinusoidal model. On the other hand, the DRW + sinusoidal model was found to be a better fit to the data than a pure DRW model in other studies (Charisi et al. 2015; D'Orazio et al. 2015b; Liu et al. 2018). In our model, it is likely that a large σ value is preferred due to the lack of variability in the *V* band. For instance, the amplitude of the *V*-band variability inferred solely from the *Swift* observations is underestimated compared to the respective amplitude inferred from the ASAS-SN data, which can plausibly be attributed to unfortunate sampling (see Section 4.2 for a detailed discussion).

Subsequently, we investigate how the assumptions in the Doppler boost model affect our results. First, we vary the amplitude ratio and repeat our tests for $A_{DB} = 1, 1.5, 3, 4, 5$.[11] In (part of) Fig. 3, we show the *p*-value as a function of σ and τ, for $A_{DB} = 3$ (top right), $A_{DB} = 4$ (bottom left), and $A_{DB} = 5$ (bottom right). For higher Doppler boost amplitudes, we cannot reject the Doppler boost hypothesis, except for a small range of σ and τ, in the case of $A_{DB} = 3$. Nevertheless, the UV/optical spectral slopes of PG1302-102, estimated in Section 3.2, are in tension with such a high Doppler boost amplitude ratio. Additionally, we also explore smaller A_{DB} values (1 and 1.5) in Fig. 3 because from the control sample in Charisi et al. (2018), we see that the expected values of this ratio range from $A_{UV}/A_{opt} = 1-2$ for typical spectral slopes. However, in Section 4.2 we discuss a potential explanation for the high value required to pass our statistical test.

An additional assumption in our fiducial model is that the DRW variability in the the optical and *UV* bands have the same amplitude ($\sigma_{UV} = \sigma_{opt}$; note that in the simulations, the DRW light curves are drawn independently in the two bands, although see also Sections 4.5 and 4.7). However, there is significant evidence that quasars have wavelength-dependent variability, with higher amplitudes at shorter wavelengths (e.g. Vanden Berk et al. 2004; Welsh, Wheatley & Neil 2011), with the variability in optical and *UV* bands correlated (Hung et al. 2016; Buisson et al. 2017). Motivated by this, we increase the amplitude of the DRW variability in the UV to reflect the intrinsic colour-variability of quasars. We repeated our tests of the Doppler boost hypothesis for $r_{noise} \equiv \sigma_{UV}/\sigma_{opt} = 2, 3, 4$; the *p*-value in each case is shown in Fig. 4. This figure shows that as the relative amplitude of the DRW is increased, the Doppler boost model is excluded for a smaller range of parameters. However, this effect is relatively less significant.

3.2 Test in other bands

Since our observations with *Swift*/UVOT cover six distinct bands, we extend the test to additional combinations of bands (in particular,

---

[11]Technically, the relative amplitude is not an assumption, but a robust prediction of the Doppler boost model if the spectral indices are known. However, it is possible that the spectral slopes vary, leading to varying values of the Doppler boost amplitude. Furthermore, if the amplitude in one band is poorly constrained, e.g. see Section 4.2, the estimate of the relative amplitude can be significantly affected.
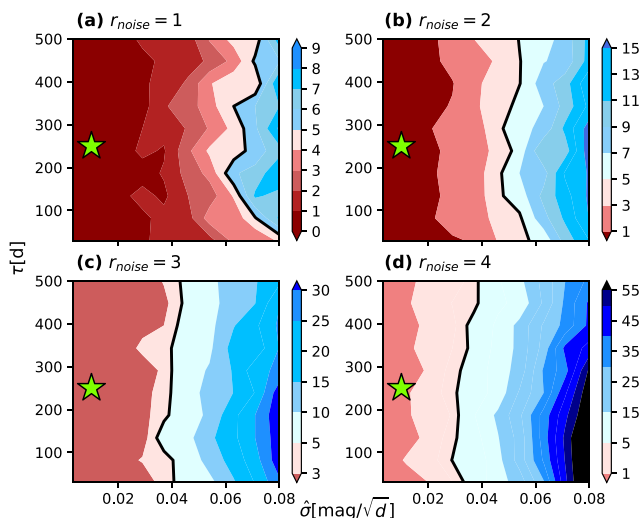
Figure 4. *P*-value (the colour bars; in unit of per cent) as a function σ and τ, for $A_{DB} = 2.17$ and with $r_{noise} = \sigma_{UV}/\sigma_{opt} = 1$ (top left), 2 (top right), 3 (bottom left), and 4 (bottom right), again considering the *Swift V* and *M*2 bands.
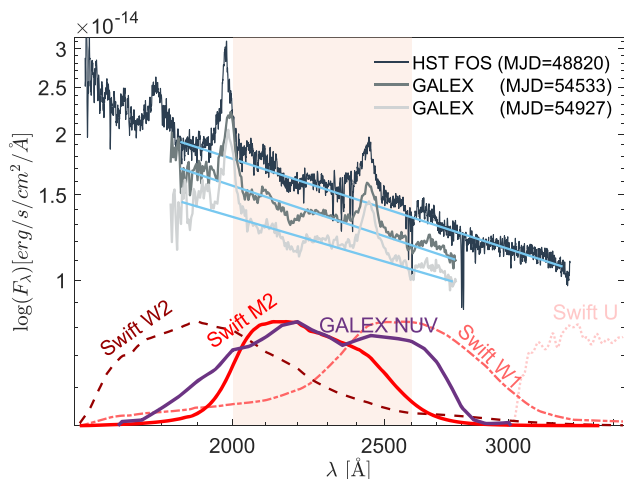

Figure 5. UV spectra from *HST* (black) and GALEX (grey and light grey). The blue lines show power-law fits to the continuum. The transmission curves of the *Swift*/UVOT (and GALEX NUV) filters are shown to delineate the wavelength coverage of each band – the transmission curves are for illustrative purposes and are not measured in flux units (*y*-axis). The shaded band indicates the wavelength range in which the near-UV spectral slope was estimated in D'Orazio et al. (2015b).

we test the model in *B* versus *M*2 and *V*/*B* versus *W*1). For this, we first calculate the spectral slopes in the remaining bands (beyond *M*2 and *V*), to predict the expected relative amplitudes A_{DB} from equation (2).

In Fig. 5, we show the UV spectra, presented in DHS15, focusing on the wavelength range covered by the four *UV* bands of *Swift*. For reference, we also show the transmission curves of the *Swift* filters and the *GALEX* near-UV filter. There are three available UV spectra (one from *HST* and two from *GALEX*), taken several hundred days apart. We fit a power law to the continuum $F_\lambda \sim \lambda^{\beta_\lambda}$ and calculate the spectral index $\alpha_\nu = -\beta_\lambda - 2$ (Table 2). Our estimate of $\alpha_\nu \sim -1$ is in agreement with the value in DHS15. In Table 2, we show the exact values obtained from each spectral fit. Fig. 5 shows that a

Table 2. UV and optical spectral slopes from fitting the continuum with a single power law.

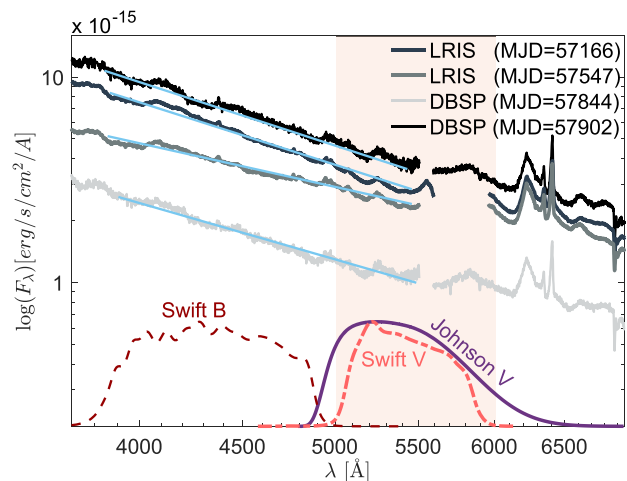|	MJD	β_λ	α_ν
UV	48820	−1.05	−0.95
	54533	−1.07	−0.93
	54927	−0.95	−1.05
	DHS15	−0.95	−1.05
Optical	57166	−3.13	1.13
	57547	−2.19	0.19
	57844	−2.83	0.83
	57902	−3.19	1.19
	DHS15	−3.10	1.10

Figure 6. Optical spectra taken with DBSP at Palomar and LRIS at Keck.

single power law can reasonably describe the continuum of PG1302-102 in almost all *UV* bands. We also see that the UV spectral index does not change significantly over time. Additionally, the available spectra cover only a small fraction of the *U* band. Therefore, we exclude this band from the analysis, since we cannot estimate the spectral index. We also exclude *W*2 because it significantly overlaps with the broad CIV line; in SMBHBs, the broad emission lines are unlikely to be associated with the mini-discs (Lu et al. 2016), but its presence in the wavelength range of *W*2 may lead to additional variability, which is not related to Doppler boosting.

As part of an ongoing effort to spectroscopically follow-up the SMBHB candidates from CRTS (Graham et al. 2015a), we have obtained four optical spectra of PG1302-102, two with the Low Resolution Imaging Spectrometer (LRIS) on the WM Keck Observatory and another two with the Double Spectrograph (DBSP) on the Palomar 200 inch telescope. In Fig. 6, we show the optical spectra (along with the transmission curves of the optical filters of UVOT and Johnson *V* band), with a power-law fit to the continuum. We summarize the estimated spectral slopes in Table 2. The continuum in optical bands (from ∼3800 to ∼5500 Å) can be successfully described by a single power law. For longer wavelengths (>5500 Å), the flux density F_λ seems to flatten, consistent with the composite quasar spectrum from Vanden Berk et al. (2001). However, because of the gap between the blue and red channels of DBSP and LRIS, the calibration of the two spectral components is slightly uncertain and thus the estimation of the slope in this part of the spectrum is challenging. We consider the value obtained from fitting the blue
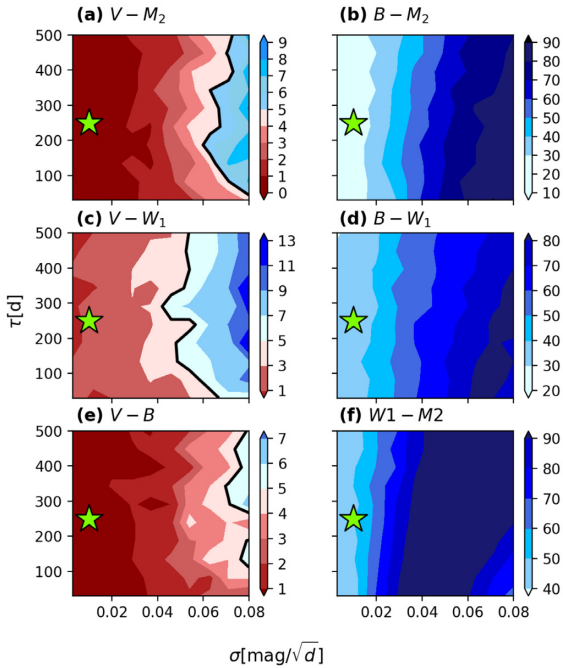
Figure 7. *P*-value (the colour bars; in unit of per cent) as a function of DRW parameters σ and τ for six combinations of independent UV ($M2$ and $W1$) and optical (V and B) bands, where $A_{DB} = 2.17$ in panels (a)–(d) and $A_{DB} = 1$ in (e) and (f), and UV/optical noise ratio $r_{noise} = 1$.

component of the spectrum to be an upper limit for the spectral slope in the V band. With the exception of the spectrum taken on MJD = 57547, the spectral index is roughly constant. However, since the spectral slope in one of the four spectra is significantly different, we cannot exclude the possibility that the spectral index may vary over time.

The spectral fits in Fig. 6 show that the same power law can describe the continuum both in V and B bands (although the continuum appears to flatten somewhat on the long-wavelength side of the V band). From Fig. 5, we find that the spectral index is similar for $M2$, $W1$, and $W2$. Therefore, we can extend the test of the Doppler boost hypothesis to other combinations of optical/UV bands, with Doppler boost amplitude ratio $A_{DB} = 2.17$ for combinations of UV–optical bands (V–$M2$, B–$M2$, V–$W1$, B–$W1$) and $A_{DB} = 1$ for optical–optical (V–B) and UV–UV bands ($M2$–$W1$), where $r_{noise} = 1$ throughout this analysis for simplicity. In Fig. 7, we show the *p*-value for the following combinations of optical and UV filters: V versus $M2$ (top left), B versus $M2$ (top right), V versus $W1$ (middle left), and B versus $W1$ (middle right). We see that, when the B band is considered, the data are consistent with the Doppler boost model for all the examined values of σ and τ. In the bottom row, we show the results of the same Doppler ratio test, but applied internally within the optical V versus B (bottom left) and UV $W1$ versus $M2$ bands. These show that the Doppler models are strongly ruled out because of the internal inconsistency within the optical bands with this model. Note that because of the flattening of the V-band continuum spectra on the long-λ side covering the V band, the Doppler boost ratio is expected to be higher when V band is involved, compared to the B band.

So far, we calculated the *p*-value of the Doppler boost hypothesis using the ratio test in all possible (six) pairwise combinations of the four bands, as shown in Fig. 7. In order to assess the Doppler boost hypothesis in all bands simultaneously, we assume that the ratio tests

are independent (if a specific band is not repeated). Therefore, there are three combinations of pairs, which cover all the bands without repetition; we can calculate the *p*-value of the full multiband test by multiplying the *p*-values of the pairwise tests [e.g. p(V/B) × p($W1$/$W2$), etc.], as shown in Fig. 8. For example, the *p*-values in Fig. 8(a) are the products of *p*-values in Fig. 7(e) and (f). Fig. 8 shows statistical lower limits of the multiband likelihoods of the Doppler model because we assumed all bands are independent. These lower limits are between 1 per cent and 2 per cent, implying that the model is ruled out at 98–99 per cent confidence. In reality, the intrinsic variability of each band is correlated; accounting for these correlations should increase the *p*-values compared to those shown in Fig. 8.

4 DISCUSSION

4.1 Data extraction–pipeline caveat

As mentioned in Section 1, we extracted the *Swift* data using the on-line interface. Most epochs in the light curve (practically, all the epochs from our follow-up program in C13 and C14) consist of multiple observations taken very close in time. In this case, the on-line pipeline provides two options for magnitude estimation; the first relies on co-adding all the available images, whereas the second uses the image with the longest exposure time. We found that the data points extracted with the different options are not always in agreement. Since the individual exposures are not separated by long time intervals, it is unlikely that the observed discrepancy is caused by quasar variability (e.g. see Caplar et al. 2017).

We devised the following tests to guide the selection of the optimal strategy for the data extraction. First, we cross-correlate the *Swift* observations with the light curve from ASAS-SN. As shown in Fig. 6, the V band of *Swift* is very similar to Johnson V band of ASAS-SN,[12] which allows for direct comparison. In Fig. 9, we show the ASAS-SN light curve superimposed with the *Swift* observations. We present the output light curves for the two data reduction options (co-added versus longest exposure, on the top and bottom panels, respectively), see Table 3. We highlight with black triangles the ASAS-SN observations that are closest in time to the *Swift* points. With the exception of the last epoch, there are nearly simultaneous observations of PG1302-102 from ASAS-SN (maximum one week apart). We see that the magnitudes from the co-added images are consistent with the ASAS-SN magnitudes within the photometric uncertainty, whereas the magnitudes from the images with the longest exposures are not in good agreement. Note that for the first two epochs, there is a single exposure and the magnitudes are identical in both light curves.

Additionally, we examined the magnitudes of nearby stars in the images of PG1302-102. We found that with co-addition the stars had almost constant magnitudes, as expected, which was not true when we opted for the longest exposure images. From the above tests, we concluded that the light curves from the co-added images are more appropriate for our analysis. Even though the reason for the discrepancy is unclear, a potential explanation is that single exposures are more susceptible to outliers. Therefore, we caution future users of the on-line pipeline about this caveat.

---

[12]The photometry of ASAS-SN is calibrated with the AAVSO Photometric All-Sky Survey catalogue, which was conducted also in Johnson V (among seven other filters).
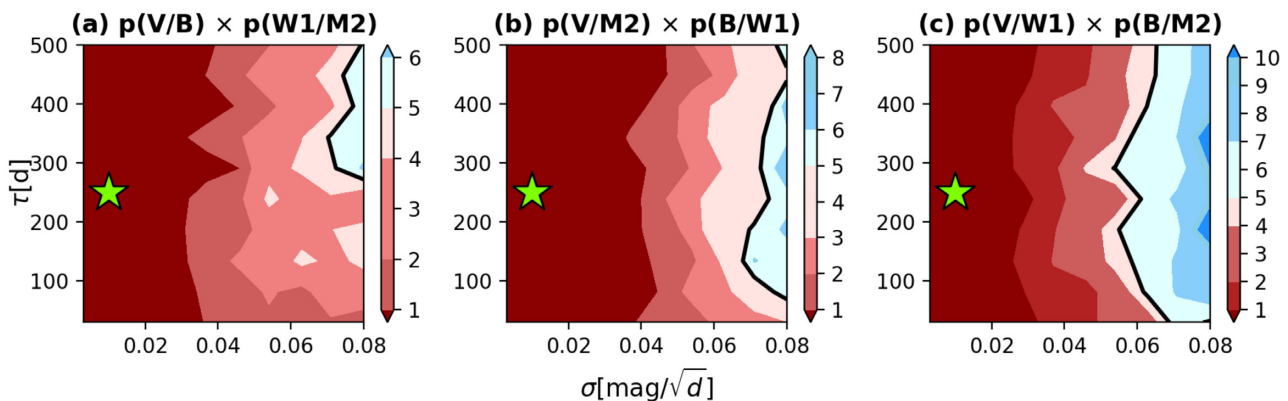
Figure 8. *P*-values (the colour bars; in unit of per cent) of three pairs of independent combinations of bands *versus* the DRW parameters, assuming Doppler amplitude $A_{DB} = 1$ for the combinations of bands in panel (a) and $A_{DB} = 2.17$ in panels (b) and (C), and UV/optical noise ratio $r_{noise} = 1$.

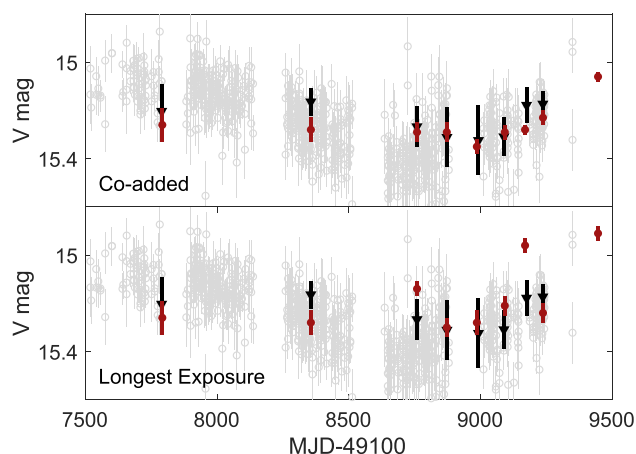**Figure 9.** Comparison between ASAS-SN and *Swift* *V*-band photometry. The ASAS-SN data points are identical in both panels and are shown in light grey, except for the points taken closest to the time of the nine *Swift* observations analysed in this paper, which are shown in black. The red data points show *Swift* photometry from co-added images (top panel) and from the longest exposure single image (bottom panel). The co-added *Swift* data are in better agreement with ASAS-SN.

4.2 Optical variability amplitude

When we examined the data in the *V* and *M*2 (or *W*1) bands, the null hypothesis tests lead us to conclude that we can exclude the fiducial Doppler boost model. The model is feasible only when the ratio of the Doppler-boost amplitudes in the two bands is high, but current estimates of the UV and optical spectral slopes are in tension with this high required ratio. On the other hand, the data are consistent with the Doppler boost model when we consider the *B*-band observations (both with *M*2 and *W*1).

A potential caveat that could explain the preference for high A_{DB}, when the test involves the *V* band can be seen from a careful examination of the light curves in Fig. 1. The amplitude of the UV variability is similar to that in DHS15, whereas the *V*-band variability, calculated solely based on the *Swift* data, is significantly smaller. The best-fitting amplitude for a sinusoid with the period and phase from DHS15 is 0.32 mag for the *M*2 band and ∼0.1 mag for the *V* band – and is reduced to only 0.028 mag if the last observation is omitted. On the other hand, from the ASAS-SN light curve, which covers the same time interval but with many more observations, the

Table 3. *Swift* *V*-band archival data for co-added and longest exposure measurements (corresponding to the data points shown in the top and bottom panels of Fig. 9, respectively). The bold-faced rows highlight the observations with multiple exposures, where these two differ. The table shows observation date in MJD, exposure time (t_{expo}) in seconds, *V*-band magnitude (*V* mag) and magnitude errors (σ_m).

	MJD	t_{expo}	*V* mag	σ_m
Co-added	56892	62	15.26	0.07
	57456	61	15.28	0.05
	57859	136	15.29	0.04
	57972	127	15.29	0.04
	58086	**214**	**15.35**	**0.03**
	58192	**170**	**15.29**	**0.093**
	58269	**496**	**15.28**	**0.02**
	58337	**566**	**15.23**	**0.03**
	58546	**520**	**15.06**	**0.02**
Long expo	56892	62	15.26	0.07
	57456	61	15.28	0.05
	57859	136	15.14	0.03
	57972	127	15.30	0.04
	58086	**112**	**15.28**	**0.05**
	58192	**92**	**15.21**	**0.04**
	58269	**137**	**14.96**	**0.03**
	58337	**135**	**15.24**	**0.04**
	58546	**136**	**14.91**	**0.03**

inferred amplitude of the sinusoid is 0.13 mag, similar to DHS15. We note that, in Section 4.1, we demonstrated that the *Swift* data points are generally consistent with the closest (in time) data points from ASAS-SN (see also top panel of Fig. 9).

Given that we base our conclusions on the small number of data points taken by *Swift*, it is likely that our results are affected by unfortunate sampling exaggerated by short-term variability of quasars (which cannot be easily accounted for in our analysis, since we assess the statistical significance of the model by simulating sinusoids). The model may be rejected, because the test is unable to reproduce the UV variations, relative to the optical, which are particularly small and thus the need for larger UV/optical Doppler boost ratios (Fig. 3), and/or larger UV noise amplitudes (Fig. 4). We note further that the *B*-band variability may be a cleaner test of the Doppler boost than the *V* band. This is because of the following. In a simple toy model of the binary nucleus of PG1302-102, the thermal emission comes from three distinct regions: (1)
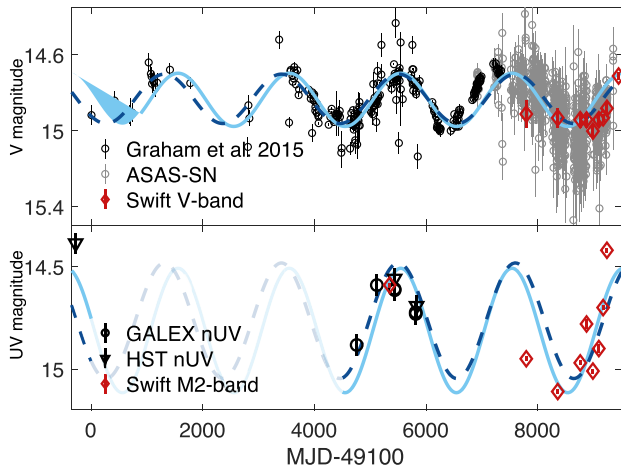
Figure 10. Optical *V*-band (top panel) and near-UV *M*2-band (bottom panel) light curve of PG1301-102, similar to Fig. 1. The prediction of the Doppler model with parameters from DHS15 is shown with a solid light-blue line. The dashed-dark-blue line represents a sinusoidal fit of the extended optical light curve, with period P = 2095 d longer than in DHS15, and the corresponding Doppler boost prediction for the UV data with A_{DB} = 2.17 in the bottom panel.

the circumprimary minidisc, (2) the circumsecondary minisdisc, and (3) the circumbinary disc. While the emission in the *B* and the *UV* bands can safely be attributed to the circumsecondary mini-disc (with small contributions from the circumprimary disc), the *V*-band luminosity may receive a significant contribution from the circumbinary disc because of the tidal truncation of the circumsecondary disc (see extended data fig. 1 in D'Orazio et al. 2015b). Since the circumbinary disc emission does not share the Doppler boost of gas bound to the secondary BH, it can add, effectively, a contribution that spoils the Doppler test.

We conclude that additional *V*-band data would be important, and could change our conclusions, rendering previously rejected models acceptable, or increasing the confidence at which the Doppler-boosted models can be ruled out. The former possibility is already demonstrated above, since the inclusion of the last observation leads to a significantly increased amplitude for the sinusoid (from 0.028 to ∼0.1). This means that even a small number of additional observations may have a profound effect in resolving the conflicting conclusions between *V*- and *B*-band tests. It is therefore crucial to continue monitoring PG1302-102 in optical and *UV* bands.

4.3 Period of PG1302-102

We tested the Doppler boost model for a fixed period and phase (P = 1994 d, $\phi = \pi$), using the parameters from DHS15. This is consistent with Liu et al. (2018)'s estimate from a light curve including additional data from ASAS-SN ($P = 2012.6^{+280}_{-220}$ d). We remind the reader that Graham et al. (2015b) had calculated a period of $P = 1884 \pm 88$ d, also consistent with both of the above estimates. Here, we examine how the precise value of the period affects our results on the multiwavelength Doppler boost signature. For this, we fit a sine wave to the extended light curve. We obtain a new best-fitting period of 2095 d, which we show in Fig. 10 (the dashed dark blue line), along with the best-fitting sinusoid from DHS15 (the solid blue line), for comparison. We also present the rescaled sinusoids, which reflect the prediction of the Doppler boost model in UV, with A_{DB} = 2.17. We see that, with the updated period, the

UV model does not fit the data equally well because the UV points are slightly out of phase.

The estimated best-fitting period is within the 1σ confidence intervals of Liu et al. (2018). We note, however, that this sinusoidal fit is not directly comparable with Liu et al. (2018) for the following reasons: (1) We fit a pure sine wave without a DRW component. (2) We consider the phase of the sinusoid as a free parameter and include it in the fit. (3) The light curve we analyse includes all the data points from Graham et al. (2015b) plus the ASAS-SN data, whereas Liu et al. (2018) examined only the data from CRTS, LINEAR, and ASAS-SN. (4) Liu et al. (2018) binned the entire light curve using wide bins of 150 d (∼100 d for the ASAS-SN light curves and 180 d for the CRTS + LINEAR light curve),[13] but we analysed all the data points without binning. (5) We employ a non-linear regression, not an MCMC analysis.

4.4 Deviations for sinusoidal variability

Equation (1) predicts that, for a circular binary, the relativistic Doppler boost will produce smooth sinusoidal variations, if: (1) the spectral indices are constant in both the optical and *UV* bands, and (2) the rest-frame luminosity in the most luminous mini-disc is constant. If any of the above conditions is not met, i.e. $\alpha_\nu \neq$ const. or $F_\nu \neq$ const., the variability will deviate from purely sinusoidal. Additional deviations may occur from the intrinsic quasar noise due to accretion on to the SMBHs, but this is taken into account with the addition of the DRW component in equation (4).

In our analysis, we assume that the ratio of the amplitudes A_{DB} is constant, i.e. the spectral indices remain unchanged through the long baseline of our observations. This seems to be a good assumption, especially in UV (Fig. 5). In the optical bands (Fig. 6), however, there is some evidence for spectral variability, since the spectral slope changes significantly in one of the four optical spectra. Additionally, quasars have a well-established trend that their spectra become bluer in their brightest phase. Therefore, it is possible that the spectral indices vary over time. The statistical test we employed, based on the ratio of pairs of observations, cannot easily incorporate changes in A_{DB}.

The null hypothesis test also assumes that the rest-frame luminosity does not vary, since we assess the statistical significance of our findings by simulating sinusoids. Nevertheless, from hydrodynamical simulations, we expect fluctuations in the mini-discs, along with significant gas motion between the two SMBHs, which can contribute to additional Doppler boost variability beyond that from the orbital motion of the binary (Tang et al. 2018). In fact, the ratio test was designed in order to incorporate such changes. Unfortunately, these effects are not well understood, and it is thus particularly challenging to develop a physically motivated model to incorporate the additional variability in the statistical analysis. We recognize that this is an important effect, and we defer its addition to future work.

Furthermore, variations in the accretion rate may also produce optical and UV variability, which may be correlated, but not simultaneous. While poorly understood even for single BHs, time lags between the optical and UV variability are possible, and could strongly influence our analysis. For example, if the accretion rate on to the binary is time variable, it may produce changes in flux

---

[13]This choice likely affects the DRW parameters rather than the sinusoid, because the bin size is much smaller than the period, but comparable to the expected τ parameter of the DRW.

that propagate inwards through the mini-discs (or the circumbinary disc), first causing a change in the optical band followed by a change in the UV. If the time lag is of the order of the orbital or thermal time at $\sim 100 GM/c^2$, where typically the emission transitions from optical to UV, for PG1302-102 one would expect correlated variations on time-scales of months to years. If instead these flux variations are mediated by viscous processes, then the time lag could be much longer, at least hundreds of years. Such a correlation between the UV and optical could help disentangle flux variations not induced by Doppler boost. Note that the expected time lag in this binary scenario is the opposite of the time lag in the regular accretion disc around a single SMBH, in which the optical follows the changes in the UV flux with minimal time lags of days (at least from cross-correlations of two well-sampled light curves in Buisson et al. 2017).

4.5 Wavelength-dependent variability of quasars

An important caveat in distinguishing the Doppler boost signature is that all quasars show wavelength-dependent variability, which can mimic the expected multiwavelength Doppler variability, especially in the sparse data, which are typically available (Charisi et al. 2018). This wavelength-dependent variability of quasars has been extensively characterized, and found to have larger amplitudes towards shorter wavelengths (Vanden Berk et al. 2004; MacLeod et al. 2010; Schmidt et al. 2012; Gezari et al. 2013; Morganson et al. 2014; Caplar et al. 2017). In particular, the recent study by Xin et al. (2020) found that, in most quasars, the near-UV and optical variability are strongly correlated, with an amplitude ratio between $2 \lesssim A_{\rm UV}/A_{\rm opt} \lesssim 3.5$. Since this encompasses the value of 2.17 expected for the Doppler model given the optical/UV spectra of PG1302-102, a concern is that this ratio can arise by chance, from stochastic multiwavelength variability.

In order to quantify how frequently the generic underlying colour-variability mimics the Doppler-induced value, it is necessary to compare the relative amplitude of optical and UV light curves $A_{\rm UV}/A_{\rm opt}$ with the expected value in the Doppler model, based on the spectral indices in the respective bands (see equation 2), for a large control sample of aperiodic quasars. This requires the availability of spectra in both bands, as well as optical and UV time-domain data (ideally sampled in both bands at the same time). Unfortunately, the number of quasars with such data are limited; Charisi et al. (2018) analysed a small sample of 42 quasars and found that the Doppler signature can arise by chance in ~ 20 per cent (40 per cent) of the cases for the near-UV (far-UV) band. This probability reflects the limited data quality of the control sample (as is also demonstrated from the increase of chance coincidence in the lower quality far-UV data), and represents only an upper limit on how frequently quasars mimic the Doppler colour variations. A larger sample of quasars with better UV + optical is needed to assess this caveat more accurately.

4.6 Constraints from future observations

An interesting question to ask is how much the evidence for or against the Doppler model may tighten with continued multiband monitoring of PG1302-102. To address this question, we generated hypothetical data representing future observations over ~ 10 yr, covering two additional cycles of periodicity, and computed the *p*-values of the Doppler model with the extended data. For simplicity, we focused on the *V* and *M*2 bands only.

In particular, we assumed that the follow-up monitoring will continue with observations similar to those in Cycles 13 and 14. We mimicked the cadence of the existing *Swift* observations, by picking consecutive epochs of future observed dates that are 122 d apart (i.e. three epochs per year), and generated a total of 33 new mock observations to cover a baseline of 10 yr. We also approximated the photometric errors for the mock *V*- and *M*2-band data by taking the average of the errors over the last seven *Swift* observations, which yields ~ 0.03 and ~ 0.01 mag, respectively.[14] Finally, we combined the additional hypothetical data with the original nine *Swift* points to construct the full new light curves.

First, we assumed that the Doppler boost model is, in fact, correct. We simulated 50 random realizations of mock *V*-and *M*2-band data, using the fiducial DB and DRW parameters from DHS15. We generated continuous DB and DRW light curves for a time period of 10 yr, downsampled these at the forecast future MJDs and added photometric uncertainty. We show an example of a hypothetical light curve in the left most panel of Fig. 11. The other two panels in Fig. 11 represent different models from the fiducial, which will be explained later in this section. We then computed the corresponding *p*-values of the mock data, following the method described in Section 2.2. We generated 1000 mock light curves to assemble the reference CDF, corresponding to the 'theoretical prediction' for the new data in the Doppler model (see Fig. 2). In this analysis, we added the new mock data points one-by-one, and re-computed the *p*-values as each of the 1, 2, ..., 33 new data points were added. For each added epoch, we calculated 50 *p*-values (one for each realization of the mock data). In Fig. 12, we show the average of the 50 *p*-values, as a function of the extension of the baseline (starting from the current constraints shown by the red triangle). The *p*-value for the DB + DRW model is shown by the topmost (dark blue) curve.

In the above exercise, we used the same model to generate and to fit the mock data – i.e. we assume that we correctly guessed the true nature of PG1302-102. Under this assumption, the expected average *p*-value, as defined in our analysis, is $\langle p \rangle = 50$ per cent; we therefore expect the *p*-values to increase and approach this value as more mock data are added. The dark blue curve in Fig. 12 shows this trend, although there are fluctuations during the additional 10 yr, caused by the stochastic nature of the DRW and random photometric errors. Additionally, we note that despite a relatively steep rise over the first additional 3 yr, the *p*-value reaches a plateau of ~ 30 per cent. These results suggest that data over an additional ~ 1 cycle of periodicity would be most useful to acquire, with relatively smaller gains thereafter.

We next make a forecast for the scenario in which the fiducial Doppler boost model is incorrect, either because the parameters we adopted differ from the true values, or because Doppler modulations are entirely absent from the true variability of PG1302-102. We generated mock data to examine examples for both of these cases. In the first case, we assumed that the true Doppler boost ratio is higher than in our fiducial model (e.g. $A_{\rm DB} = 3$ instead of 2.17). In the second case, we assumed that PG1302-102's variability is caused by DRW alone. The middle and right-hand panel of Fig. 11 demonstrate examples of each case, along with the fiducial model. In both cases, we expect that as new data are added, the *p*-values would begin to decrease, since the wrong model is being fit to more and more data. Our results, shown by the light blue and dark

---

[14]For the estimation of the typical photometric error, we omitted the earliest two *Swift* observations, prior to our observing program in Cycles 13 and 14, because they have large errors due to short exposure times.
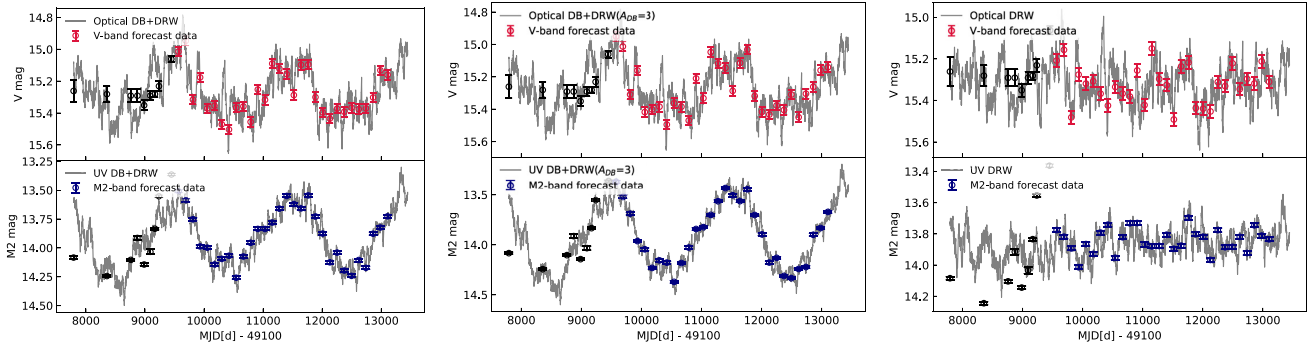
Figure 11. Example hypothetical light curves over upcoming ∼10 yr, for each of the three cases explained in Section 4.6; (1) the fiducial DB and DRW model with $A_{DB} = 2.17$ dominates the variability of PG1302 (left); (2) DB + DRW model has higher Doppler amplitude ratio, $A_{DB} = 3$ (middle); and (3) DB is absent from the system and DRW model dominates the true variability (right). In all three scenarios, the DRW amplitude ratio is fixed at 1 (i.e. $r_{noise} = 1$). The black points with the error bars are the existing nine *Swift* observations in optical (top panels) and UV (bottom panels). The red and dark blue points with the error bars are the hypothetical optical and UV data, respectively.
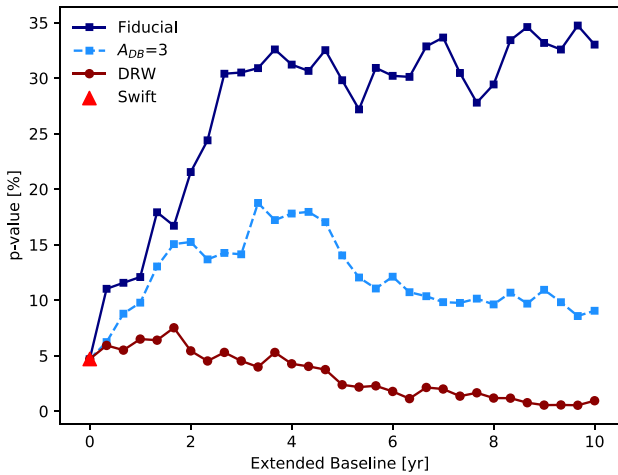

Figure 12. *P*-values inferred when the fiducial model is fit to three different hypothetical future data sets with extended baselines. The red triangle denotes the original nine *Swift* points. The dark blue curve is inferred from mock data generated in the fiducial model itself. The light blue curve assumes that the true light curve has a larger Doppler amplitude ratio ($A_{DB} = 3$). The dark red curve corresponds to future mock data consisting of pure DRW variability.

red curves in Fig. 12, indeed show these trends in the long run. However, while in the latter case (when the true variability is a pure DRW), the *p*-values decrease monotonically, the former case, in which the Doppler amplitude ratio is guessed incorrectly, shows a temporary increase over the first additional cycle. These results lead us to conclude that converging on the correct model will require monitoring PG1302-102 for at least two additional cycles of the periodicity. On the other hand, just ≈ two additional years of data appears very useful to distinguish between the pure DRW and the DRW + DB hypotheses.

4.7 Future work

We have described several caveats and limitations of the currently available data that prevent us from definitively ruling out the multiband observations of PG1302-102 are consistent with the Doppler boost model. Here, we delineate potential improvements in the observing strategy that will allow us to tackle each of the above issues.

First, we saw that we reached different conclusions from the analysis of *V*- and *B*-band observations; in Section 4.2, we discussed the possibility that our results are affected by the small amplitude of the *Swift V*-band light curve, e.g. compared to ASAS-SN. This may be caused by unfortunate sampling, given that we examine a small number of simultaneous optical/UV observations. If the light curve were to include a larger number of observations (e.g. twice as many points), the light curve, and thus our results, would be less prone to such effects.

Another possibility/limitation in the fiducial values taken in this study is the assumption that the relative amplitudes are fixed and equal to 2.17. As discussed above, if the spectral indices change over time, the relative amplitude will reflect this change. If the photometric observations are accompanied by spectral measurements, practically, there will be no free parameters in the model. With simultaneous multiband photometric and spectroscopic observations, even a small number of data points can provide more definitive conclusions.

Finally, we incorporated the stochastic variability of quasars by adding the DRW variability of optical and UV wavelengths. We assume that these deviations are incoherent (we draw independent realizations for the optical and UV DRW variability). Even though this is beyond the scope of this paper, a comprehensive analysis of the covariance between optical and UV light curves of quasars is necessary to validate this choice (see Xin et al. 2020).

5 SUMMARY

In this paper, we presented simultaneous observations of PG1302-102 with the *Swift* satellite in two UV and two optical bands. This is a significant enhancement to the previously available observations, which consisted of a smaller number of UV data points that were not taken simultaneously with optical data and only in one optical and one *UV* band. We performed a statistical analysis to test the Doppler boost hypothesis, which predicts that the UV variability should track the optical, but with a ∼2.2 times higher amplitude. From the analysis of nine simultaneous observations from *Swift*, we found that

(i) The new light curves roughly trace the sinusoidal trends expected from the Doppler boost model.

(ii) The multiwavelength data are consistent with relativistic Doppler boost when the *B*-band versus *M*2 (and *W*1) data are considered.

(iii) The *V*-band versus *M*2 (and *W*1) data could still be consistent with the Doppler boost model, but only if either the ratio of UV/optical variability is larger than expected from the spectral slopes, the stochastic variability makes large contribution in the UV, or the UV/optical spectral slopes vary.

(iv) A potential explanation for the rejection of the Doppler boost model (with the *V*-band data) is that the sparse new optical data from *Swift* underestimate the true optical variability. Comparison with the light curve from ASAS-SN suggests that this is likely.

(v) If we consider all four bands simultaneously, combining independent pairs of bands, the Doppler model is disfavoured.

(vi) Additional, simultaneous optical and UV observations tracking another cycle of PG1302-102's proposed period should lead to a definitive conclusion.

ACKNOWLEDGEMENTS

REFERENCES

Artymowicz P., Lubow S. H., 1996, ApJ, 467, L77+
Barth A. J., Stern D., 2018, ApJ, 859, 10
Begelman M. C., Blandford R. D., Rees M. J., 1980, Nature, 287, 307
Bon E. et al., 2016, ApJS, 225, 29
Buisson D. J. K., Lohfink A. M., Alston W. N., Fabian A. C., 2017, MNRAS, 464, 3194
Burke-Spolaor S. et al., 2019, A&AR, 27, 5
Caplar N., Lilly S. J., Trakhtenbrot B., 2017, ApJ, 834, 111
Charisi M., Bartos I., Haiman Z., Price-Whelan A. M., 2015, MNRAS, 454, L21
Charisi M., Bartos I., Haiman Z., Price-Whelan A. M., Graham M. J., Bellm E. C., Laher R. R., Márka S., 2016, MNRAS, 463, 2145
Charisi M., Haiman Z., Schiminovich D., D'Orazio D. J., 2018, MNRAS, 476, 4617
Comerford J. M., Pooley D., Gerke B. F., Madejski G. M., 2011, ApJ, 737, L19
Cuadra J., Armitage P. J., Alexander R. D., Begelman M. C., 2009, MNRAS, 393, 1423
De Rosa A. et al., 2019, New Astronomy Reviews, 86, 101525
D'Orazio D. J., Di Stefano R., 2018, MNRAS, 474, 2975
D'Orazio D. J., Loeb A., 2017, ApJ, 863, 185
D'Orazio D. J., Haiman Z., MacFadyen A., 2013, MNRAS, 436, 2997
D'Orazio D. J., Haiman Z., Duffell P., Farris B. D., MacFadyen A. I., 2015a, MNRAS, 452, 2540
D'Orazio D. J., Haiman Z., Schiminovich D., 2015b, Nature, 525, 351
D'Orazio D. J., Haiman Z., Duffell P., MacFadyen A., Farris B., 2016, MNRAS, 459, 2379
Dorn-Wallenstein T., Levesque E. M., Ruan J. J., 2017, ApJ, 850, 86
Farris B. D., Duffell P., Macfadyen A. I., Haiman Z., 2014, ApJ, 783, 12
Gezari S. et al., 2013, ApJ, 766, 60
Gold R., Paschalidis V., Ruiz M., Shapiro S. L., Etienne Z. B., Pfeiffer H. P., 2014, Phys. Rev. D, 90, 104030
Graham M. J. et al., 2015a, MNRAS, 453, 1562
Graham M. J. et al., 2015b, Nature, 518, 74
Haehnelt M. G., Kauffmann G., 2002, MNRAS, 336, L61
Haiman Z., Kocsis B., Menou K., 2009, ApJ, 700, 1952
Hung T. et al., 2016, ApJ, 833, 226
Ivezić Ž., Connolly A., Vanderplas J., Gray A., 2014, Statistics, Data Mining and Machine Learning in Astronomy. Princeton Univ. Press, Princeton, NJ
Jun H. D., Stern D., Graham M. J., Djorgovski S. G., Mainzer A., Cutri R. M., Drake A. J., Mahabal A. A., 2015, ApJ, 814, L12
Kelley L. Z., Haiman Z., Sesana A., Hernquist L., 2019, MNRAS, 485, 1579
Kochanek C. S. et al., 2017, PASP, 129, 104502
Komossa S., Burwitz V., Hasinger G., Predehl P., Kaastra J. S., Ikebe Y., 2003, ApJ, 582, L15
Kormendy J., Ho L. C., 2013, ARA&A, 51, 511
Kozłowski S., 2017, A&A, 597, A128
Kozłowski S. et al., 2010, ApJ, 708, 927
Li Y.-R. et al., 2019, ApJS, 241, 33
Liu T., Gezari S., Miller M. C., 2018, ApJ, 859, L12
Liu T. et al., 2019, ApJ, 884, 36
Lu K.-X., Li Y.-R., Bi S.-L., Wang J.-M., 2016, MNRAS, 459, L124
MacFadyen A. I., Milosavljević M., 2008, ApJ, 672, 83
MacLeod C. L. et al., 2010, ApJ, 721, 1014
Morganson E. et al., 2014, ApJ, 784, 92
Mushotzky R. F., Edelson R., Baumgartner W., Gand hi P., 2011, ApJ, 743, L12
Nixon C. J., Cossins P. J., King A. R., Pringle J. E., 2011, MNRAS, 412, 1591
Qian S. J., Britzen S., Witzel A., Krichbaum T. P., Kun E., 2018, A&A, 615, A123
Rodriguez C., Taylor G. B., Zavala R. T., Peck A. B., Pollack L. K., Romani R. W., 2006, ApJ, 646, 49
Roedig C., Dotti M., Sesana A., Cuadra J., Colpi M., 2011, MNRAS, 415, 3033
Roedig C., Sesana A., Dotti M., Cuadra J., Amaro-Seoane P., Haardt F., 2012, A&A, 545, A127
Ryan G., MacFadyen A., 2017, ApJ, 835, 199
Schmidt K. B., Rix H.-W., Shields J. C., Knecht M., Hogg D. W., Maoz D., Bovy J., 2012, ApJ, 744, 147
Sesana A., Haiman Z., Kocsis B., Kelley L. Z., 2018, ApJ, 856, 42
Shappee B. J. et al., 2014, ApJ, 788, 48
Shi J.-M., Krolik J. H., 2015, ApJ, 807, 131
Smith K. L., Mushotzky R. F., Boyd P. T., Malkan M., Howell S. B., Gelino D. M., 2018, ApJ, 857, 141
Tang Y., MacFadyen A., Haiman Z., 2017, MNRAS, 469, 4258
Tang Y., Haiman Z., MacFadyen A., 2018, MNRAS, 476, 2249
Timmer J., Koenig M., 1995, A&A, 300, 707
Vanden Berk D. E. et al., 2001, AJ, 122, 549
Vanden Berk D. E. et al., 2004, ApJ, 601, 692
Vanderplas J., Connolly A., Ivezić Ž., Gray A., 2012, in Conference on Intelligent Data Understanding (CIDU). p. 47
Vaughan S., Uttley P., Markowitz A. G., Huppenkothen D., Middleton J., Alston W. N., Scargle J. D., Farr W. M., 2016, MNRAS, 461, 1
Welsh B. Y., Wheatley J. M., Neil J. D., 2011, A&A, 527, A15
Xin C., Charisi M., Haiman Z., Schiminovich D., 2020, MNRAS, 495, 1403
Zheng Z.-Y., Butler N. R., Shen Y., Jiang L., Wang J.-X., Chen X., Cuadra J., 2016, ApJ, 827, 56
Zhu X.-J., Thrane E., 2020, preprint (arXiv:2004.10944)

APPENDIX A: *SWIFT* DATA

This appendix includes the *Swift* observational data for all six *UVOT* bands, along with their errors.

Table A1. *Swift* Data. Column 1: MJD; Columns 2, 4, 6, 8, 10, 12: *V*, *B*, *W*1, *M*2, *W*2-band magnitudes; Columns 3, 5, 7, 9, 11, 13: *V*, *B*, *W*1, *M*2, *W*2-band magnitude errors.

MJD	*V*		*B*		*U*		*W*1		*M*2		*W*2	
56892	15.26	0.07	15.38	0.03	14.17	0.03	14.10	0.03	14.08	0.01	14.12	0.02
57456	15.28	0.05	15.27	0.03	14.25	0.03	14.14	0.03	14.24	0.01	14.17	0.02
57859	15.29	0.04	15.52	0.03	14.23	0.02	14.22	0.01	14.10	0.01	14.27	0.02
57972	15.29	0.04	15.42	0.03	14.21	0.01	13.88	0.02	13.91	0.02	13.90	0.02
58086	15.35	0.03	15.57	0.02	14.41	0.02	14.20	0.02	14.14	0.01	14.28	0.02
58192	15.29	0.03	15.45	0.02	14.20	0.01	14.01	0.02	14.03	0.02	14.00	0.02
58269	15.28	0.02	15.37	0.02	14.17	0.01	13.89	0.01	13.83	0.01	13.87	0.01
58337	15.23	0.03	15.31	0.01	14.11	0.01	13.79	0.01	13.55	0.01	13.72	0.01
58546	15.06	0.02	15.12	0.01	13.90	0.01	13.37	0.01	13.36	0.01	13.26	0.01

This paper has been typeset from a TEX/LATEX file prepared by the author.